Sensors and Actuators B 173 (2012) 772–780

Contents lists available at SciVerse ScienceDirect

Sensors and Actuators B: Chemical

journal homepage: www.elsevier.com/locate/snb

# Highly sensitive and selective hydrogen single-nanowire nanosensor

O. Lupan [a,b,c,*], L. Chow [a,**], Th. Pauporté [b], L.K. Ono [a], B. Roldan Cuenya [a], G. Chai [a]

[a] Department of Physics, University of Central Florida, Orlando, FL 32816-2385, USA
[b] Chimie-Paristech, Laboratoire d'Électrochimie, Chimie des Interfaces et Modélisation pour l'Énergie (LECIME), UMR-CNRS 7575, 11 rue P. et M. Curie, 75231, Paris, cedex 05, France
[c] Department of Microelectronics and Semiconductor Devices, Technical University of Moldova, 168 Stefan cel Mare Blvd., Chisinau MD-2004, Republic of Moldova

ARTICLE INFO

*Article history:*
Received 12 April 2012
Received in revised form 25 July 2012
Accepted 28 July 2012
Available online 3 August 2012

*PACS:*
81.05.Dz
81.07.Bc
81.16.Be
07.07.Df
81.16.−c
85.35.−p

*Keywords:*
Cd-doped
ZnO nanowire
Nanosensor
Gas response
Selective
Hydrogen

ABSTRACT

Metal oxides such as ZnO have been used as hydrogen sensors for a number of years. Through doping, the gas response of zinc oxide to hydrogen has been improved. Cadmium-doped ZnO nanowires (NWs) with high aspect ratio have been grown by electrodeposition. Single doped ZnO NWs have been isolated and contacted to form a nanodevice. Such nanosystem demonstrates an enhanced gas response and selectivity for the detection of hydrogen at room temperature compared to previously reported $H_2$ nanosensors based on pure single-ZnO NWs or multiple NWs. A dependence of the gas response of a single Cd–ZnO nanowire on the NW diameter and Cd content was observed. It is shown that cadmium-doping in single-crystal zinc oxide NWs can be used to optimize their response to gases without the requirement of external heaters. The sensing mechanisms responsible for such improved response to hydrogen are discussed.



## 1. Introduction

Hydrogen sensors are widely used in combustion systems of automobiles to monitor pollution, certain types of bacterial infections, as well as in the petroleum, chemical, or semiconductor industries [1,2]. The potential applications of semiconductor nanocrystals and quantum dots for chemical sensing have been pointed out [3], and tremendous progress has been made in recent years in the synthesis and assembly of such materials [4–6]. In addition, new physical and chemical properties can be obtained upon nanocrystal doping [5,7–12], enabling new applications in the fields of nano-electronics and nano-optoelectronics [3,4,12,13]. Previous reports discussed different aspects of doping for nanocrystals [4,5,7–12]. In the case of ZnO, direct chemical methods for the synthesis of doped nanowires (NWs) such as thermal evaporation, chemical vapor deposition, or solid-state synthetic techniques were found to require annealing temperatures above 500 °C [12–15]. Aqueous solution routes including electrochemical deposition constitute alternative methods for low temperature doping [11,16–25] of nanowires and nanorods, with the added advantages of its simplicity, fast implementation, and low cost. In addition, the electrochemical method allows the control of the dopant concentration, the orientation and density of the nanorods formed by adjusting deposition potentials, current densities, temperature, and/or salt concentrations [19–25]. Cadmium is an excellent dopant for ZnO, because Zn and Cd belong to the same group in the Periodic Table, and they both occupy the same type of lattice sites in wurtzite structures [22,25]. Thus, the stable wurtzite ZnO structure is expected to be preserved upon Cd-doping at low concentrations [22,24,25].

One-dimensional nanostructures show great potential for nanodevice applications [26–31] based on their large surface to volume ratio and controlled flow of confined charge carriers. For example, Cd-doped ZnO NWs have been used in light-emitting devices, thin-film transistors, and sensing nanodevices [22,24,26]. Many nano-ZnO-based $H_2$ sensors have been demonstrated [28–31]. For example, hydrogen-selective sensing in nano-zinc oxide based

* Corresponding author at: Department of Physics, University of Central Florida, Orlando, FL 32816-2385, USA. Tel.: +1 407 823 2333; fax: +1 407 823 5112.
** Corresponding author. Tel.: +1 407 823 2333; fax: +1 407 823 5112.
*E-mail addresses:* lupan@physics.ucf.edu, lupanoleg@yahoo.com (O. Lupan), Lee.Chow@ucf.edu (L. Chow), thierry-pauporte@chimie-paristech.fr (Th. Pauporté), guangyuchai@yahoo.com (G. Chai).

0925-4005/$ – see front matter © 2012 Elsevier B.V. All rights reserved.
http://dx.doi.org/10.1016/j.snb.2012.07.111

sensors was observed on: pure and Pt-coated multiple ZnO nanorods [32,33], ZnO nanorod arrays and networks [34,35], single nanorod/nanowire ZnO [28–30], and $SnO_2$-coated ZnO nanorods [36]. However, for industrial production purposes, an inexpensive and efficient synthesis process is required [21–23]. Although, previous reports of single pure ZnO nanowire/nanorod-based $H_2$ sensors showed the promise of such devices in commercial sensing applications, their relative slow response and recovery times are major drawbacks for their implementation in an industrial setting. Future demands on chemical nano-sensors require enhanced sensitivity, selectivity, stability, and faster gas responses. Improvements in the performance of single-nanowire sensors can be achieved via doping or surface functionalization.

In the present work we used an electrochemical method for the synthesis of Cd-doped ZnO NWs with high aspect ratios. By using a focused ion beam, an individual ZnO NW was integrated into a nanodevice structure, and its response to hydrogen at room temperature measured. Our device displayed an improved performance compared to previously reported $H_2$ nanosensors based on pure single-ZnO NWs. In particular, by doping the ZnO NWs, a reduction of their operation temperature and enhancement of their gas response and selectivity were observed.

## 2. Experimental

Cadmium-doped ZnO nanowire arrays were grown on F-doped tin oxide (FTO) film supported on a glass substrate, with a sheet resistance of 10 Ω/sq, using an electrochemical deposition (ECD) process [22–24]. The following parameters were used during the electrodeposition: an electrical potential of −1 V versus SCE, a total charge per unit area of $-10\,C\,cm^{-2}$, a deposition temperature of 92 °C [22,24,37], a $CdCl_2$ concentration in the ZnO deposition bath of 0, 2 or 6 microM and a total growth time of 150 min. After ECD, the samples were rinsed with DI water and dried in air. Subsequently, the samples were subjected to thermal annealing in air at 300 °C for 11 h to relax the ZnO lattice.

Scanning electron microscopy (SEM) images were acquired with an Ultra 55 Zeiss FEG at an acceleration voltage of 10 kV. The synthesized structures were characterized with a high-resolution X-ray diffractometer (Siemens D5000) operated at 40 kV and 45 mA using Cu $K_{\alpha 1}$ radiation (λ = 1.5406 Å). Secondary ion mass spectrometry (SIMS) was used for the analysis of the Cd content because of its excellent sensitivity and depth resolution [37]. SIMS measurements were carried out with a Physical Electronics ADEPT 1010 quadrupole analyzer with a 3 keV $Cs^+$ primary beam at 60° from normal direction. The typical primary beam current was 25 nA. The primary beam was rastered over a 300 μm by 300 μm area, with the detection of negative secondary ions from an area of 100 μm by 100 μm at the center of the rastered area. Details of the experimental procedures can be found in previous reports [37].

Further analysis of the chemical composition of the synthesized samples was conducted via X-ray photoelectron spectroscopy (XPS). For this purpose, a hemispherical electron energy analyzer (Phoibos 100, SPECS GmbH) and an Al $K_\alpha$, (1486.6 eV) monochromatic X-ray source (XR50M, SPECS GmbH) were used. Sample charging was corrected using the binding energy (BE) of adventitious carbon as reference (C-1s peak = 285 eV).

The nanosensors were built by contacting a single ZnO NW on the substrate template (glass with Al contacts as contact electrodes) by using the metal deposition function of our FIB. The single-NW contacts were imaged using FESEM. Consistent resistance data from several single nanowire devices were obtained. Additional details on the connection of very thin ZnO NW (80–100 nm in diameter) using FIB/SEM are given in our recent work [28]. Also, it should be pointed out that during fabrication, the single Cd–ZnO NW was exposed to the FIB beam for less than 8 min. The enhanced radiation hardness of ZnO NWs as compared to bulk ZnO layers was also reported in Refs. [28,38]. This method can be applied to the fabrication of single-NW contacts from a variety of radiation-resistant materials. The characteristic $H_2$ response of a nanosensor structure was studied at room temperature (RT, 22 °C). The measuring apparatus consisted of a closed quartz chamber connected to a gas flow system [28]. The humidity of the gas mixture was kept at about 65% relative humidity (RH) at RT. The concentration of test gases was measured using a pre-calibrated mass flow controller. Hydrogen and air were introduced to a gas mixer via a two-way valve using separate mass flow controllers. The test gases were allowed to flow to a test chamber with a sensor holder, in which the nanosensor was placed. By monitoring the output voltage across the nanorod-based sensor, the changes in the resistance were measured in air and in a test gas. A computer with suitable LabView interface handled the acquisition of the data. All measurements were performed in a quasi-steady state.

## 3. Results and discussion

Figure 1a shows a scanning electron microscopy SEM image of a quasi-aligned high aspect ratio Cd-doped ZnO NW array grown by electrodeposition on a FTO substrate. These NWs have uniform lengths of 2–3 μm and diameters of 50–200 nm. The NWs are well facetted and have hexagonal cross-sections exhibiting {1 0 0} planes on the sides (Fig. 1a inset). The length/width aspect ratio of the doped ZnO NWs is about 30, which is 50% higher than that of pure ZnO NWs under the same growth conditions [22].

A TEM image of an individual nanowire with uniform diameter is presented in Fig. 1b. A high-resolution TEM image taken from the edge of the sample and the associated electron diffraction pattern (SAED) indicate that the ZnO NWs have a single crystal structure, do not display any noticeable defects, and are oriented along the ⟨0 0 0 1⟩ *c*-axis (Fig. 1c). The measured lattice spacing (*c* = 5.2055 Å) corresponds to that of ZnO crystalline planes. However, ZnO and CdO can normally be found in two different stable crystal structures – wurtzite and rocksalt, respectively, which complicates the fabrication of single-phase structures in a broad compositional range [39]. Previous detailed analysis of diffraction and photoluminescence (PL) data revealed that the wurtzite single-phase stability range is likely to be as narrow as 0–2% Cd in ZnCdO [39]. Figure 1c presents a selected area electron diffraction (SAED) pattern of a Cd–ZnO NW grown by ECD. The SAED pattern and HRTEM image reveal that the Cd–ZnO nanowires are uniform and single crystalline. According to our TEM observation, we conclude that highly crystalline Cd–ZnO NWs with hexagonal structure can be successfully synthesized at low temperature by electrodeposition as previously reported [22,24,25]. An X-ray diffraction pattern from this sample (XRD not shown here) shows predominant (0 0 2) diffraction peaks [22]. The lattice constants of pure bulk ZnO are *a* = 3.249 Å and *c* = 5.206 Å [22], and those of pure ZnO nanorods (wurtzite structure) *a* = 3.2506 Å, *c* = 5.2055 Å [30]. However, larger lattice parameters (a = 3.2507 Å and c = 5.207 Å) were obtained for the doped ZnO NWs for Cd concentrations in the electrolyte of 2 and 6 μM [22].

The chemical composition of the NWs was investigated by SIMS. Figure 2 shows Zn, Cd and Sn signals from the Cd (6 μM)-doped ZnO NW on FTO versus the sputtering time. The Cd count rate seems to closely follow the Zn count rate over most of the investigated sample depth. This is an indication that the Cd dopant has been evenly incorporated into the ZnO NW structure. As expected, no correlation between the Cd and Sn (from the FTO substrate) count rates was observed, and a gradual increase in the Sn signal is observed as a function of the sputtering time until saturation is reached. The experiments suggest that Cd doping is about 1 at. % [22,24].

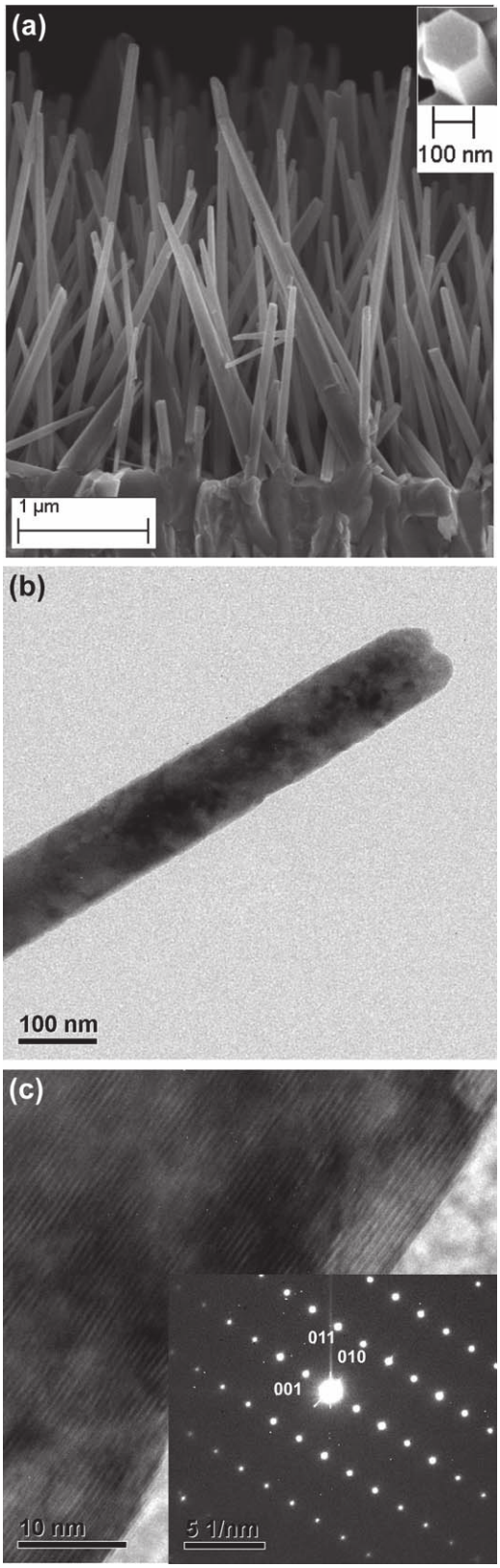


**Fig. 1.** (a) SEM micrograph (side view) of ZnO–Cd (6 μM $CdCl_2$ in the electrolyte) nanowires electrodeposited on an FTO substrate, (b) TEM image of the ZnO–Cd nanowire revealing the surface morphology and (c) HRTEM image of the ZnO–Cd nanowire. The insert shows an SAED selected area electron diffraction pattern.

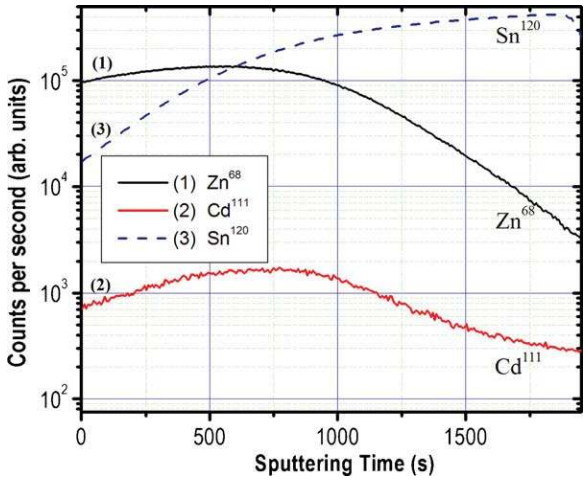


**Fig. 2.** SIMS measurements of Cd (6 μM)-doped ZnO. The dashed curve (Sn) corresponds to the FTO substrate.

XPS analysis was conducted to determine the presence of the Cd dopants and their chemical state inside the ZnO matrix [40–42]. Figure 3 displays XPS spectra from the (a) Zn-2p and (b) Cd-3d core level regions of the Cd-doped ZnO NWs. The Zn-2p region shows a doublet at 1021.7 eV and 1044.8 eV corresponding to the Zn-$2p_{3/2}$ and $2p_{1/2}$ core levels. The Cd-3d region also shows a doublet tentatively assigned to cationic Cd ($Cd^{\delta+}$, $3d_{5/2}$ = 405.6 eV and $3d_{3/2}$ = 412.4 eV) (Fig. 3(b)). Literature Refs. [41,42] report the following BEs for Cd-$3d_{5/2}$: 404.8 eV for $Cd^0$, 404.0 eV for $Cd^{2+}$ in CdO, and 404.6 eV for $Cd^{2+}$ in $Cd(OH)_2$. Nevertheless, it should be noted that those

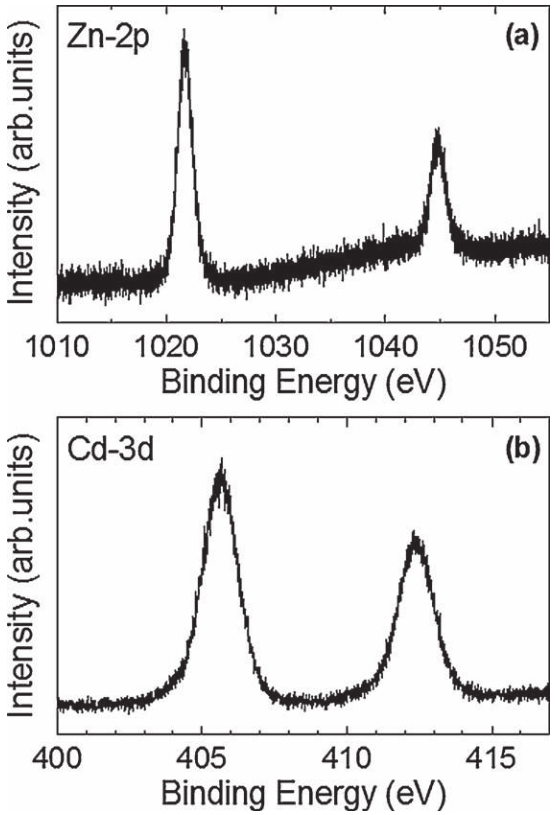


**Fig. 3.** XPS spectra (Al $K_\alpha$ = 1486.6 eV) corresponding to the (a) Zn-2p and (b) Cd-3d core level regions of Cd-doped ZnO nanorods supported on a FTO-coated glass substrate.

references correspond to bulk-Cd samples, contrary to the case of our Cd-dopants, which could be present on our samples as ions in ternary compound $Zn_{1-x}Cd_xO$ ($3d_{5/2}$ = 404.6–405.3 eV) [14,43–46] or small clusters [47,48].

As was pointed out above and in previous reports [28–36], there is an increasing interest in $H_2$ nanosensors because hydrogen is a potential source of alternative clean energy. However, the majority of commercial hydrogen sensors suffer from high power consumption, since they operate at relatively high temperatures (about 300 °C), which may complicate their integration in wireless sensor networks. Therefore, in order to develop high performance hydrogen sensors based on ZnO NW, high operation temperatures must be avoided not only to reduce power consumption, but also to prevent the reduction of ZnO in the $H_2$ atmosphere [28,49]. At this stage there are no reports on metal-doped individual NWs or Cd-doped-ZnO-based sensors made from a single NW.

Individually separated Cd-doped ZnO NWs were released from an array of as-grown NWs (see Fig. 1a) by sonication in ethanol, and subsequently transferred to a $SiO_2$-coated Si substrate or by a direct contact technique of the sample with a clean Si wafer. Several devices were fabricated using Cd–ZnO NWs with lengths between 2 and 3 μm and radii between 40 nm and 100 nm, which showed reproducible electrical responses. The current–voltage ($I$–$V$) curves of the nanosensors measured at 300 K show a linear behavior. The NW dark-resistance of ~6 kΩ in air at atmospheric pressure is assigned to oxygen molecules and water molecules adsorbed on the NW surface, which are expected to capture free electrons [28] as well as to contribute to the protonic conduction on the NW surface. As mentioned in the experimental part, the humidity of the gas mixture was kept at about 65% RH at 22 °C. The higher dark-resistance ~10 kΩ in dry air is assigned to oxygen molecules adsorbed on the NW surface, which are expected to capture more free electrons. According to Ref. [28], the gas response is defined as: $S \approx |\Delta R/R_{air}|$, where $|\Delta R| = |R_{air} - R_{gas}|$ and $R_{air}$ is the resistance of the sensor in air and $R_{gas}$ is the resistance in the test gas. Figure 4a shows the transient response of ZnO and Cd-doped ZnO-nanowire sensors (curves 1 and 2, respectively) of about 90 nm diameter upon exposure to 100 ppm of $H_2$ gas at RT. As can be seen in Fig. 4a (curve 2), both, response time ($\tau_r$) and recovery times ($\tau_f$) ($\tau = |t_{90\%} - t_{10\%}|$) were very fast for the Cd–ZnO NW, taking 14 and 11 s for 90% full response and recovery, respectively. By comparing curve 2 for Cd–ZnO NW with curve 1 for pure ZnO NW, a larger and quicker gas response was observed in the case of the doped NW sensor. The changes in the resistance of the sensor after exposure to hydrogen return to within 10% of the initial value in about 11 s for the doped sample. This is explained by the presence of adsorbed gas molecules, which are desorbed from the surface of the doped ZnO NW faster than in the case of a pure ZnO NW. Usually, operation at elevated temperature or UV light pulses are used in order to desorb the gas species from the surface of the sensor material [28]. In our case, the larger surface-to-volume ratio of the single-crystalline NWs offers potential to improve the gas response and selectivity for hydrogen. The proposed gas sensing mechanism will be discussed in detail below.

Figure 4b shows a comparison of the gas response of a pure- and Cd-doped ZnO NW sensors (90 nm in diameter). It can be seen that by doping ZnO with cadmium the gas response to $H_2$ at RT is improved. The insert in Fig. 4b shows the single-NW contacted by FIB. Figure 4c demonstrates the dependence of the gas response on the diameter of the Cd–ZnO NW sensors. The highest gas response (about 274%) was obtained from a sensor based on a single Cd (6 μM)-doped ZnO NW with a 90 nm diameter. For comparison, 140 nm and 200 nm ZnO NWs show a lower response to $H_2$, namely, less than 68% and 40%, respectively. Our results demonstrate the validity of thin doped ZnO NWs as $H_2$ sensors for low temperature operation conditions. Additionally, the power consumption of

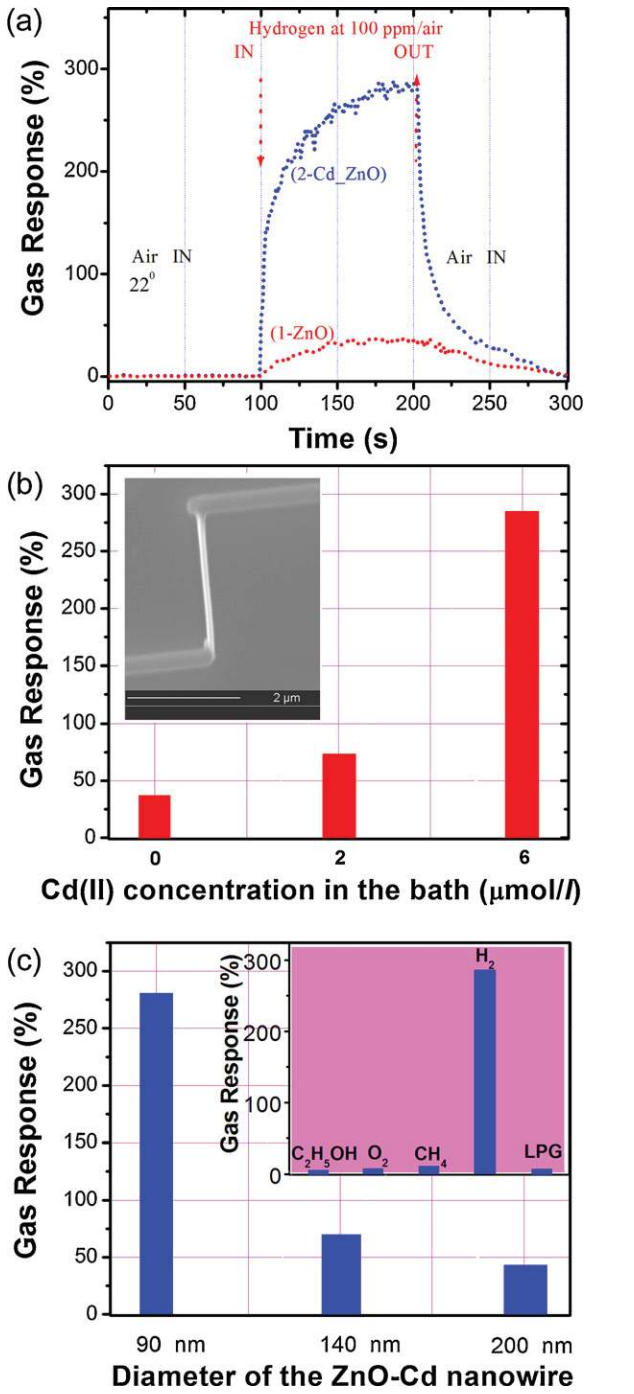


**Fig. 4.** Room temperature gas responses of nanosensors based on a single pure ZnO NW and a ZnO–Cd (6 μM) NW of ~90 nm diameter versus (a) time, and (b) the concentration of [Cd] (0–6 μM $CdCl_2$) in the electrolyte. For the Cd-doped ZnO NW, the gas response is also shown as a function of the NWs' diameter (90, 140 and 200 nm) (c). In all cases, a 100 ppm $H_2$ gas pulse was used. The insert in (b) shows an SEM image of a single ZnO–Cd (6 μM) NW connected in a nanosensor configuration. The insert in (c) shows the gas response of the single Cd–ZnO NW-sensor to different gases (100 ppm $H_2$, 200 ppm others). All measurements were performed at RT.

such nanosensors is ~5 nW, which makes it very competitive for integration in wireless nanosensors networks. The existence of a depletion space charge region at the NW surface [28,50] can qualitatively explain the dependence of the gas response on the NW diameter (Fig. 4c).

Relative humidity (RH) measurements were also conducted with the ZnO NW under different conditions using a saturated salt

solution method described elsewhere [51–53]. A humidity detection mechanism for ZnO pellets with different electrical contacts was reported by Traversa and Bearzotti [53]. The electrical resistance of the ZnO-Cd nanodevice structures was found to decrease slightly with increasing RH from 12 to 97%. It should be also considered that a Pico-Ammeter was used as power source and a nano-V meter to monitor the voltage drop on the sensor. The NW can act as heating as well as a sensing element. Thus, the increased in the locally temperature ($T \sim 120\,^{\circ}C$, evaluated according to [54–56]), due to self-generated heat, might contribute to the desorption of adsorbed molecules (including water) in ambient conditions. In such case, conductivity changes could be a result of electronic conduction [53]. Chemisorbed water molecules donate electrons and the resistance varies. As reported before, at RT the conductivity of ceramic semiconducting materials is due to a combination of electronic and protonic (ionic) pathways, unless moisture cannot effectively condense on the surface ($T > 100\,^{\circ}C$) [51]. Since our NWs act as heating elements, we can speculate that the ionic-type mechanism does not likely occur. Instead, the electronic mechanism, which takes place at higher temperatures [53], should dominate. However, at the same time we observed a humidity-induced degradation of the ZnO:Cd NW-based sensor structure at relatively high RH values. This could be due to the diffusion and reaction of mobile $H^+$ protons generated by dissociation of water at the NW surface [52,57]. These results suggest the idea to use some protective approaches for ZnO NW-based sensor. The reproducibility in this work was defined as the repeatability of the same sensor working with a humidity cycle of low–high–low–high conditions. It was observed that the Cd-doped ZnO sensor showed a better gas response than the undoped sensor. More details about the impact of humidity on ZnO-based nanosensors will be presented in a forthcoming paper.

Recently, Kim et al. [58] reported that adsorbed H atoms on ZnO NW surfaces, as for example Zn-H(a) and O-H(a), would desorb molecularly as $H_2$ at two different temperatures, 330 K and 450 K, respectively, reflecting their adsorption strengths. The more strongly bound H atoms on the oxygen surface are removed completely after heating above 685 K, which leads to restoring the clean ZnO surface [59]. Chan and Griffin [60] reported that adsorbed H(a) desorbed from Zn sites at ~319 K, in good agreement with results reported by Kim et al. [58]. These results can support our experimental observations as well as proposed sensing mechanism.

In order to test the selectivity to $H_2$ of our Cd–ZnO nanosensor, the response to $C_2H_5OH$, $O_2$, $CH_4$ and LPG (liquefied petroleum gas) have also been investigated and summarized in Fig. 4c (insert). We can see that the ZnO nanosensor's response to 200 ppm LPG and 200 ppm $CH_4$ is much lower in comparison with its gas response to hydrogen. These data show the high selectivity of the fabricated nanosensor for $H_2$ and the high prospect of thin doped ZnO NWs as material for nanoscale sensors operating at room temperature.

Next, we would like to discuss our proposed sensing mechanism for a single ZnO NW doped with Cd as compared to a pure ZnO NW. The factors influencing gas sensing properties of zinc oxide NW and their fundamental mechanisms are still under debate. Figure 5 summarizes the factors governing the sensing performance of single ZnO NW sensors. Such discussion can be extended to other metal oxide material nanowires as well. These are: (1) the diameter ($D_{NW}$) and aspect/ratio of the individual NWs [28,30], (2) gas induced changes in the depletion region [61,62], (3) donor impurities in the NWs [63], (4) the surface potential [64], (5) adsorption/desorption enthalpy $E_{des}$ [65], (6) surface functionalization or charged surface states *Ns* [66,67], (7) temperature of operation [68], and (8) ambient relative humidity [52,69]. Figure 5 (central drawing) schematically displays a cross-sectional view of a single ZnO NW. Here, two regions can be distinguished: (i) the central part (red hexagon in Fig. 5) is a region called conduction channel, where the electronic

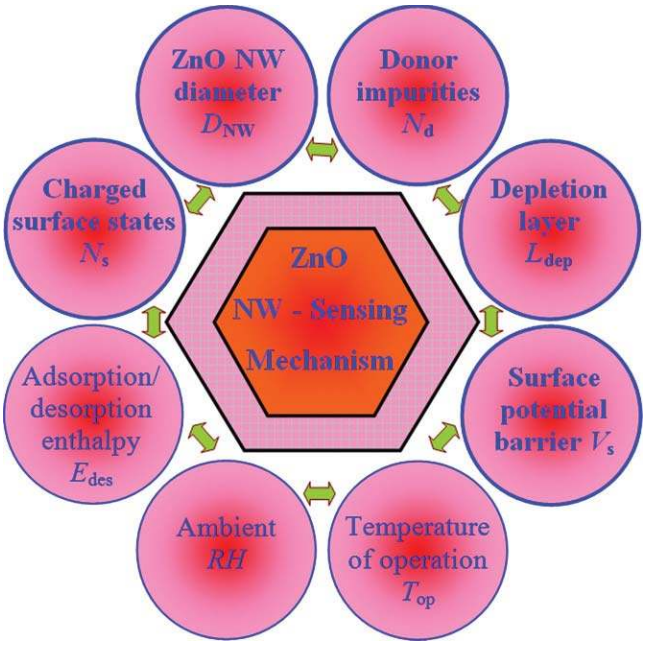


**Fig. 5.** Schematic representation of the major factors influencing the sensing mechanism of a doped single-NW ZnO sensor.

concentration is high; and (ii) the external hexagon surrounding area, also known as depletion region, where the electron concentration is much lower. Such region (cross-section of the NW) can be a partly or completely depleted layer, depending on the ratio between the diameter of the NW ($D_{NW}$) and the Debye length $\lambda_D$. In the depletion layer, the mobility of the electrical charge carriers' is much lower than in the central region due to potential barriers at the NW surface [28]. The conduction process takes place in the central region of the NW, which is much more conductive than the surrounding surface depletion layer.

A better understanding and a better control of the factors (Fig. 5) influencing the gas sensing properties is expected to lead to solutions for enhancing the gas response and selectivity of single-NW ZnO-nanosensors. Our experimental results, reveal that the main contributions to the sensing behavior of the NWs are their diameter $D_{NW}$ and aspect ratio, the depletion layer $L_{dep}$, surface potential and dopant concentration (see Fig. 5). Recently, we demonstrated that by decreasing the NW diameter, the response of single ZnO NWs to UV light and $H_2$ molecules can be largely improved [28]. Additional details related to the sensing mechanism have been described previously in Refs. [28,30]. In the present work, in addition to tuning the NW gas response by changing its diameter, it is demonstrated that the sensitivity can also be enhanced by introducing dopants into the ZnO wurzite structure.

The gas response of the resistive sensors under ambient conditions is given by the following equation [28]:

$$S = \left|\frac{G_g - G_a}{G_g}\right| \times 100\% = \left|\frac{4}{D}(\lambda_{D(a)} - \lambda_{D(g)})\right| \times 100\% \quad (1)$$

where $G_g$ and $G_a$ are the conductance of ZnO NWs in $H_2$ gas and in air ambient, respectively, $\lambda_D$ is the Debye length/radius. It can be seen that *S* depends on $\lambda_D$ and $1/D$.

The extent of the space-charge layer, which controls the electrical conductivity in the ZnO NW depends on the Debye length and the interfacial potential energy. The thickness of the depleted region, *L* is given by [70]:

$$L = \lambda_D \left(\frac{eV_s}{kT}\right)^{1/2}, \quad (2)$$

$$\text{where} \quad \lambda_D = \left(\frac{\varepsilon kT}{2\pi e^2 N_d}\right)^{1/2} \tag{3}$$

is the Debye screening length and

$$V_s = \frac{2\pi Q_s^2}{\varepsilon N_d} = \frac{2\pi(qN_s)^2}{\varepsilon N_d} \tag{4}$$

is the interfacial potential, $Q_s$ is the surface charge density, $\varepsilon$ is the dielectric constant, $N_d$ is is the concentration of donor impurity (charge carrier-concentration), $q$ is the charge of the surface state, $N_s$ is the density of charged surface states, $k$ is the Boltzmann constant, and $T$ is the absolute temperature. Thus the dependence of the thickness of the depleted region can be given as: $L \sim V_s^{1/2}$, $L \sim Q_s$, and $L \sim N_s$.

In Fig. 6 (top) we can see the schematic energy band diagram in the radial direction of a single ZnO NW and a Cd-ZnO NW indicating the depletion region at the surface, the surface band bending and the quasi-neutral core region of radius $r$ in the central part of the NW. Figure 6 (bottom) presents structural models of the conduction mechanism of single ZnO and Cd–ZnO NWs in air. The parameter $x$ denotes the depth from the surface, $qV_s$ the potential barrier at the surface, and $qV_{(x)}$ the depth profile of the potential energy of the electrons. Since, $V_s$ is the potential drop across the depletion layer, $E_c$ is the lower edge of the conduction band, and $E_F$ is the Fermi level. In the left drawing (thicker NWs) it can be seen that the depletion layer does not influence the conduction channel as much as in the case of the thinner ZnO:Cd NWs (right drawing). In the latter example, the changes of the thickness of the depletion layer have a greater effect on the conduction channel, which leads to higher responses, in accordance with our experimental observations (Fig. 4). At the same time, it has to be considered that for a thin ZnO NW (50–100 nm), a Debye length of 20–50 nm is estimated from $d = (2\varepsilon_{ZnO}\varepsilon_0 V_s/qn_e)^{1/2}$ assuming $n_e$ of about $10^{18}$ cm$^{-3}$ and $V_s$ ranging from 0.1 to 3 V [50]. Such Debye length is comparable to the NW dimensions. For pure NWs with a diameter of 50–100 nm, the charge depletion region encompasses the entire NW, and flat-band conditions take place (see Fig. 6 middle drawing). For a high purity stochiometric ZnO NW, $\lambda_{D(a)}$ can be very large due to the decrease of the charge-carrier concentration. In this case, the position of the Fermi level shifts away from the band gap throughout the entire NW (see Fig. 6, middle drawing); the equilibrium between free electrons and ionized vacancies is achieved, and electrons move without the interference of the electrostatic barrier [61]. If a surface state is present below $E_F$ under the flat band condition, which applies to the NW in the radial direction, the electrons will be transferred from the $E_c$ to these surface states and charge transfer will occur until $E_F$ becomes constant throughout the surface and the interior of the NW (equilibrium state). Electrons will be distributed homogeneously in the volume of the NW and current flow cannot be varied significantly by adsorbed $H_2$ molecules on the surface (especially at very low concentration ppm or ppb). On the other hand, for metals or degenerate semiconductors, $\lambda_{D(a)}$ is comparable to the dimension of the atom, which makes it possible to use only ultrathin layers as sensing material. Such ultrathin structures could however generate problems because of the stability of their connections.

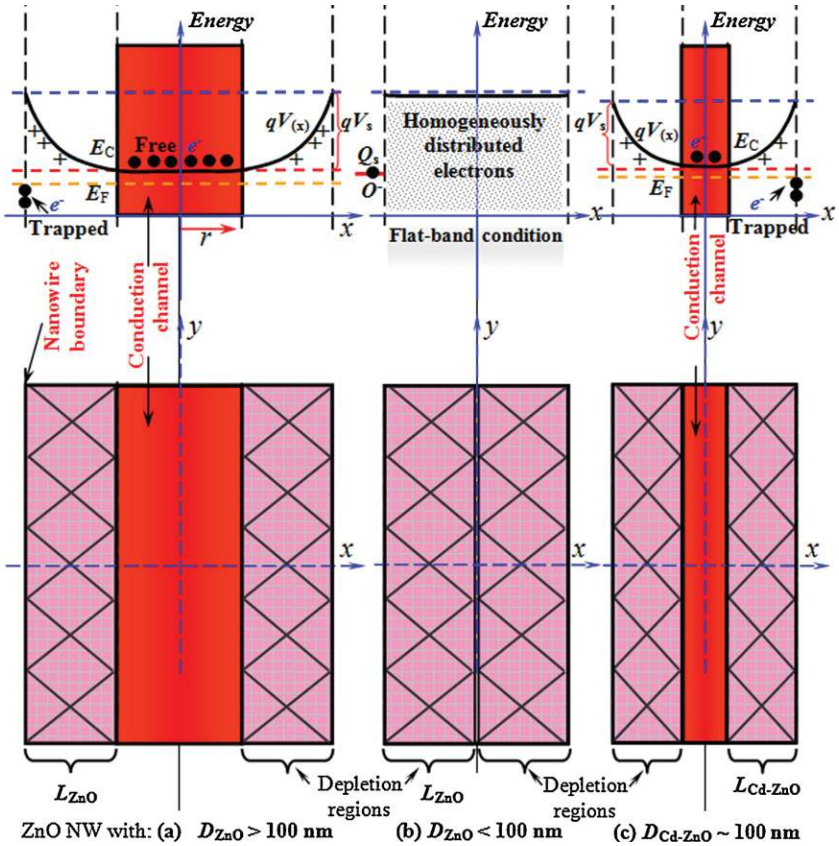


**Fig. 6.** Energy band diagram in the radial direction (up) and structural (down) models of the conduction mechanism of single ZnO and Cd–ZnO nanowire in air. $x$ – denotes depth from the surface. $L$ – denotes the depletion layer at the surface. $q$ is elemental charge of electron. $qV_s$ is the potential barrier at the surface and $qV_{(x)}$ is the depth profile of the potential energy of electrons. (up) Schematic energy band models in the radial direction of a nanowire indicating the depletion region at the surface and the quasi-neutral core region of radius $r$ in the central part of the NW. $V_s$ is the electric potential drop across the depletion layer, $E_c$ is the lower edge of the conduction band, and $E_F$ is the Fermi level. (down) Structural representation of a cross sectional view of the nanowires along its length: (a) pure ZnO NW with diameter $D > 100$ nm; (b) pure ZnO NW with diameter $D < 100$ nm and (c) doped ZnO NW with diameter $D \sim 100$ nm.

In this situation, controlled doping (the density of the conduction electrons $n \sim N_d$) or functionalization of the surface is a good approach to tune $\lambda_D$ (or depletion region, see Eq. (2)) and get enhanced gas response from ZnO NWs. This is the reason why it is important to dope ZnO NW and to control the position of the Fermi level inside the bandgap. Thus, it is possible to control sensitivity, selectivity and response time of a thinner doped NW.

According to Eqs. (1)–(3), an enhancement of the $H_2$ response can be realized by controlling the geometric factor (4/D), electronic characteristics ($\varepsilon\varepsilon_0/en_0$), and band bending ($V_{Sa}^{1/2} - V_{Sg}^{1/2}$) due to adsorption of gas on the ZnO NW surface. We can see from the above Eq. (2,3,4) that $L \sim Q_s$, $L \sim N_s$, $L \sim N_d^{-1}$, it depends on the charge of the surface state ($Q_s$), the density of charged surface states ($N_s$), and the concentration of donor impurities ($N_d$). This can be done by doping, which is the present case, or by modulating the operation temperature, which is not desirable for $H_2$ sensors on single ZnO NWs as discussed above. It was reported that the concentration of the *n*-type charge carriers increases with increasing Cd content [71]. Experimental evidences show that the source of the *n*-type conductivity in Cd-doped ZnO is related to Cd incorporation. However, Cd incorporation in ZnO, an isovalent doping, does not create a new donor level, which means that the only possible source of *n*-type carriers are the native defects or their complexes in the ZnCdO alloy [72]. Cd incorporation can change the state of native defects, such as the formation energy and the transition energy level, which induces an increase of the carrier concentration in the ZnCdO alloy. Another way is to make use of geometric parameters, and of doping at the same time, as was realized in our experiments. By using different NW diameters and different dopant concentrations, sensors with different gas response characteristics can be produced.

Due to of the Fermi level pinning at the $O^-$ level at the surface of the NW, the conduction band $E_c$ and valence band $E_v$ are bent upward at the surface as shown schematically in Fig. 6 (top). Electrons prefer the inner part of the NW, holes tend to migrate to the surface. As can be seen in the middle drawing of Fig. 6 for the pure ZnO NW, the small NW diameter leads to a complete charge depletion at a critical diameter, with unchanged surface barrier height for electrons in the $E_c$. The surface depletion layer of NWs with the same diameter *d*, but with different doping concentrations is different, as illustrated in Fig. 6 (bottom). We consider that the doping concentration of the left and middle NWs (Fig. 6) is lower than that of the right one. For wire diameters above the critical diameter, the recombination barrier is defined by the surface Fermi-level pinning. For thinner wires, the depletion region is too small to build up such a large potential difference, and the recombination barrier is smaller. Thus, the smaller barrier yields to a shorter lifetime of the carriers and therefore, a lower current and a faster response. Below the critical diameter, the current shows an exponential dependence on the NW diameter. For larger diameters, the dependence becomes linear. Increasing the doping concentration reduces the thickness of the surface depletion layer of the NW and the critical diameter ($D_c$), as shown in Fig. 6. The determination of the critical diameter by electrical or optoelectrical measurements thus allows the evaluation of the doping concentration of the NW, as will be shown in a forthcoming paper.

Thus, the current flow through the conduction channel in a NW can be controlled and consequently, the gas response. In cases where the width of the conduction channel is thinner (closer to critical value $D_c$), a better control of the charge carrier flow and of the gas response can be achieved.

For NWs with smaller diameters [28], a larger fraction of the atoms are found at the surface, and can participate in surface reactions. For thinner NWs the depletion region length is comparable to the NW radius, and the electronic properties are more influenced by adsorption–desorption processes at the surface. To improve the response and recovery times of NW-based sensors it is needed to enhance the adsorption–desorption kinetics by control of the operation temperature, including the self-heating approach [54–56], or by doping. The doping of ZnO NWs contributes to the control of the extent of the surface depletion region in the NW, which must be kept small so that the single NW is not completely depleted. Therefore, a relatively quasi-neutral core region is desired to channel current down to the contact. The doping level in our Cd–ZnO NWs was estimated to be $10^{20}$ $cm^{-3}$ based on photoluminescence spectroscopy measurements performed in our laboratory, yielding an expected depletion width of ~30 nm. We believe that the control of the doping, NW diameter, and self-heating temperature can help to improve its gas response and selectivity. These results indicate that the surface depletion has a significant influence on the electronic transport behavior of the ZnO NWs, since the depletion width is comparable to the NW diameter. This explains why the operation mode of ZnO NW devices can be controlled by the modulation of surface states through surface morphology engineering and size control.

## 4. Conclusions

Nanoscale sensors based on a single Cd-doped ZnO NW were fabricated using focused ion beam. Our device sensitivity and response time to $H_2$ (down to 100 ppm), and good selectivity (poor response to $CH_4$, $C_2H_5OH$, $O_2$, LPG and ammonia) are significantly improved in comparison with previous results of pure ZnO NWs.

A dependence of the gas response of single Cd–ZnO NWs on their diameter was observed. In particular, NWs with a diameter of 90 nm showed higher gas response. Additionally, the gas response was shown to depend on the Cd-doping, and to be significantly improved as compared to previous related reports for undoped ZnO. Adding 6 μM $CdCl_2$ in the electrolyte during ECD permits to grow NWs with improved hydrogen response. Furthermore, their low power consumption (<5 nW at 2 mV), makes them suitable for use in portable devices without the need of external microheaters [61,73]. The fact that our nanosensors, require extremely low power to operate, represents an important advance in power efficiency and nano-miniaturization. This is an important step forward toward low power and fast zinc oxide gas sensing nano-devices. In summary, we have demonstrated that cadmium-doping in single-crystal zinc oxide nanowires can be used to optimize their response to gases without the requirement of external heaters.

## Acknowledgements

BRC acknowledges the financial support from the National Science Foundation (NSF-DMR-0906562). Dr. Lupan acknowledges the CNRS for support as an invited scientist at the LECIME-ENSCP, UMR7575, Paris.

## References

[1] T. Hübert, L. Boon-Brett, G. Black, U. Banach, Hydrogen sensors – a review, Sensors and Actuators B 157 (2011) 329–352.
[2] F. Rumiche, H.H. Wang, J.E. Indacochea, Development of a fast-response/high-sensitivity double wall carbon nanotube nanostructured hydrogen sensor, Sensors and Actuators B 163 (2012) 97–106.
[3] X. Wang, Y. Wang, D. Aberg, P. Erhart, N. Misra, A. Noy, A. Hamza, J. Yang, Batteryless chemical detection with semiconductor nanowires, Advanced Materials 23 (2010) 117–121.
[4] D.J. Norris, A.L. Efros, S.C. Erwin, Doped nanocrystals, Science 319 (2008) 1776–1779.
[5] S.C. Erwin, L. Zu, M.I. Haftel, A.L. Efros, T.A. Kennedy, D.J. Norris, Doping semiconductor nanocrystals, Nature 436 (2005) 91–94.

[6] H. Zeng, J. Cui, B. Cao, U. Gibson, Y. Bando, D. Golberg, Electrochemical deposition of ZnO nanowire arrays: organization, doping, and properties, Science of Advanced Materials 2 (3) (2010) 336–358.

[7] Doped Nanomaterials and Nanodevices, 3-volume Set, Edited by Wei Chen, University of Texas at Arlington, USA American Editor, Journal of Nanoscience and Nanotechnology, USA, February 2010, p. 800, Hardcover, ISBN: 1-58883-110-8.

[8] L. Chow, O. Lupan, H. Heinrich, G. Chai, Self-assembly of densely packed and aligned bilayer ZnO nanorod arrays, Appl. Phys. Lett. 94 (2009), 163105.

[9] H. Gong, J.Q. Hu, J.H. Wang, C.H. Ong, F.R. Zhu, Nano-crystalline Cu-doped ZnO thin film gas sensor for CO, Sensors and Actuators B 115 (1) (2006) 247–251.

[10] O. Lupan, S. Shishiyanu, V. Ursaki, H. Khallaf, L. Chow, T. Shishiyanu, V. Sontea, E. Monaico, S. Railean, Synthesis of nanostructured Al-doped zinc oxide films on Si for solar cells applications, Solar Energy Materials and Solar Cells 93 (2009) 1417–1422.

[11] J.B. Cui, U.J. Gibson, Electrodeposition and room temperature ferromagnetic anisotropy of Co and Ni-doped ZnO nanowire arrays, Applied Physics Letters 87 (2005) 133108.

[12] M.T. Chen, M.P. Lu, Y.J. Wu, J. Song, C.Y. Lee, M.Y. Lu, Y.C. Chang, L.J. Chou, Z.L. Wang, L.J. Chen, Near UV LEDs made with in situ doped p–n homojunction ZnO nanowire arrays, Nano Letters 10 (2010) 4387–4393.

[13] Q.H. Li, Q. Wan, Y.G. Wang, T.H. Wang, Abnormal temperature dependence of conductance of single Cd-doped ZnO nanowires, Applied Physics Letters 86 (2005) 263101.

[14] S.M. Zhou, X.H. Zhang, X.M. Meng, S.K. Wu, S.T. Lee, Fabrication of large-scale ultra-fine Cd-doped ZnO nanowires, Materials Research Bulletin 41 (2) (2006) 340–346.

[15] F. Wang, B. Liu, C. Zhao, S. Yuan, Synthesis of $Zn_{1-x}Cd_xO$ bramble-like nanostructures, Materials Letters 63 (15) (2009) 1357–1359.

[16] D. Mocatta, G. Cohen, J. Schattner, O. Millo, E. Rabani, U. Banin, Heavily doped semiconductor nanocrystal quantum dots, Science 332 (6025) (2011) 77–81.

[17] T. Singh, T.J. Mountziaris, D. Maroudas, On the transition-metal doping efficiency of zinc oxide nanocrystals, Applied Physics Letters 97 (2010) 073120.

[18] Z. Haibo, J. Cui, B. Cao, U. Gibson, Y. Bando, D. Golberg, Electrochemical deposition of ZnO nanowire arrays: organization, doping, and properties, Science of Advanced Materials 2 (3) (2010) 336–358.

[19] M.A. Thomas, J.B. Cui, Electrochemical growth and characterization of Ag-doped ZnO nanostructures, Journal of Vacuum Science and Technology, B 27 (2009) 1673.

[20] J.B. Cui, Y.C. Soo, T.P. Chen, Low-temperature growth and characterization of Cl-doped ZnO nanowire arrays, Journal of Physical Chemistry C 112 (12) (2008) 4475–4479.

[21] O. Lupan, L. Chow, L.K. Ono, B.R. Cuenya, G.Y. Chai, H. Khallaf, S. Park, A. Schulte, Synthesis and characterization of Ag- or Sb-doped ZnO nanorods by a facile hydrothermal route, Journal of Physical Chemistry C 114 (2010) 12401–12408.

[22] O. Lupan, T. Pauporte, T. Le Bahers, I. Ciofini, B. Viana, High aspect ratio ternary $Zn_{1-x}Cd_xO$ nanowires by electrodeposition for light-emitting diode applications, Journal of Physical Chemistry C 115 (2011) 14548–14558.

[23] H. El Belghiti, T. Pauporté, D. Lincot, Mechanistic study of ZnO nanorod array electrodeposition, Physica Status Solidi A 205 (2008) 2360–2364.

[24] T. Pauporté, O. Lupan, B. Viana, Tunable electroluminescence from low-threshold voltage LED structure based on electrodeposited $Zn_{1-x}Cd_xO$-nanorods/p-GaN heterojunction, Physica Status Solidi A 209 (2012) 359–363.

[25] G.R. Li, W.X. Zhao, Q. Bu, Y.X. Tong, A novel electrochemical deposition route for the preparation of $Zn_{1-x}Cd_xO$ nanorods with controllable optical properties, Electrochemistry Communications 11 (2009) 282–285.

[26] J. Zhou, Y. Gu, P. Fei, W. Mai, Y. Gao, R. Yang, G. Bao, Z.L. Wang, Flexible piezotronic strain sensor, Nano Letters 8 (9) (2008) 3035–3040.

[27] O. Lupan, T. Pauporté, B. Viana, Low-voltage UV-electroluminescence from ZnO-nanowire array/p-GaN light-emitting diodes, Advanced Materials 22 (2010) 3298–3302.

[28] O. Lupan, V.V. Ursaki, G. Chai, L. Chow, G.A. Emelchenko, I.M. Tiginyanu, A.N. Gruzintsev, A.N. Redkin, Selective hydrogen gas nanosensor using individual ZnO nanowire with fast response at room temperature, Sensors and Actuators B 144 (1) (2010) 56–66.

[29] S.N. Das, J.P. Kar, J.H. Choi, T.I. Lee, K.J. Moon, J.M. Myoung, Fabrication and characterization of ZnO single nanowire-based hydrogen sensor, Journal of Physical Chemistry C 114 (3) (2010) 1689–1693.

[30] O. Lupan, G. Chai, L. Chow, Novel hydrogen gas sensor based on single ZnO nanorod, Microelectronic Engineering 85 (11) (2008) 2220–2225.

[31] R. Khan, H.-W. Ra, J.T. Kim, W.S. Jang, D. Sharma, Y.H. Im, Nanojunction effects in multiple ZnO nanowire gas sensor, Sensors and Actuators B 150 (2010) 389–393.

[32] H.T. Wang, B.S. Kang, F. Ren, L.C. Tien, P.W. Sadik, D.P. Norton, S.J. Pearton, Jenshan Lin, Hydrogen-selective sensing at room temperature with ZnO nanorods, Applied Physics Letters 86 (2005) 243503.

[33] L.C. Tien, H.T. Wang, B.S. Kang, F. Ren, P.W. Sadik, D.P. Norton, S.J. Pearton, J. Lin, Electrochem room-temperature hydrogen-selective sensing using single Pt-coated ZnO nanowires at microwatt power levels, Solid-State Letters 8 (9) (2005) G230.

[34] C.S. Rout, A.R. Raju, A. Govindaraj, C.N.R. Rao, Hydrogen sensors based on ZnO nanoparticles, Solid State Communications 138 (3) (2006) 136.

[35] J. Huh, J. Park, G.T. Kim, J.Y. Park, Highly sensitive hydrogen detection of catalyst-free ZnO nanorod networks suspended by lithography-assisted growth, Nanotechnology 22 (2011) 085502.

[36] L.C. Tien, D.P. Norton, B.P. Gila, S.J. Pearton, Hung-Ta Wang, B.S. Kang, F. Ren, Detection of hydrogen with $SnO_2$-coated ZnO nanorods, Applied Surface Science 253 (10) (2007) 4748–4752.

[37] O. Lupan, T. Pauporté, L. Chow, B. Viana, F. Pellé, L.K. Ono, B. Roldan Cuenya, H. Heinrich, Effects of annealing on properties of ZnO thin films prepared by electrochemical deposition in chloride medium, Applied Surface Science 256 (6) (2010) 1895–1907.

[38] A. Burlacu, V.V. Ursakii, V.A. Skuratov, D. Lincot, T. Pauporté, H. Elbelghiti, E. Rusu, I.M. Tiginyanu, The impact of morphology upon the radiation hardness of ZnO layers, Nanotechnology 19 (2008) 215714.

[39] V. Venkatachalapathy, A. Galeckas, M. Trunk, T. Zhang, A. Azarov, A. Yu Kuznetsov, Understanding phase separation in ZnCdO by a combination of structural and optical analysis, Physical Review B 83 (2011) 125315.

[40] O. Lupan, T. Pauporté, B. Viana, Low-temperature growth of ZnO nanowire arrays on p-silicon (1 1 1) for visible-light-emitting diode fabrication, Journal of Physical Chemistry C 114 (35) (2010) 14781–14785.

[41] S.W. Gaarenstroom, N. Winograd, Initial and final state effects in the ESCA spectra of cadmium and silver oxides, Journal of Chemical Physics 67 (1977) 3500.

[42] J.S. Hammond, S.W. Gaarenstroom, N. Winograd, X-ray photoelectron spectroscopic studies of cadmium- and silver–oxygen surfaces, Analytical Chemistry 47 (1975) 2193–2199.

[43] F.Z. Wang, B. Liu, C. Zhao, S.C. Yuan, Synthesis of $Zn_{1-x}Cd_xO$ bramble-like nanostructures, Materials Letters 63 (2009) 1357.

[44] U.N. Maiti, P.K. Ghosh, S.F. Ahmed, M.K. Mitra, K.K. Chattopadhyay, Structural, optical and photoelectron spectroscopic studies of nano/micro ZnO:Cd rods synthesized via sol–gel route, Journal of Sol–Gel Science and Technology 41 (2007) 87–92.

[45] F.Z. Wang, H.P. He, Z.Z. Ye, L.P. Zhu, H.P. Tang, Y. Zhang, Raman scattering and photoluminescence of quasi-aligned ternary ZnCdO nanorods, Journal of Physics D: Applied Physics 38 (2005) 2919.

[46] S.M. Zhou, X.M. Meng, X.H. Zhang, X. Fan, K. Zou, S.K. Wu, S.T. Lee, Large-scale fabrication and characterization of Cd-doped ZnO nanocantilever arrays, Micron 36 (2005) 55.

[47] M.S. Bootharaju, T. Pradeep, Uptake of toxic metal ions from water by naked and monolayer protected silver nanoparticles: an X-ray photoelectron spectroscopic investigation, Journal of Physical Chemistry C 114 (2010) 8328.

[48] S. Gorer, J.A. Ganske, J.C. Hemminger, R.M. Penner, The size-selective electrochemical/chemical synthesis of sulfur-passivated cadmium sulfide nanocrystals on graphite, Journal of the American Chemical Society 120 (1998) 9584.

[49] O. Lupan, G.A. Emelchenko, V.V. Ursaki, G. Chai, A.N. Redkin, A.N. Gruzintsev, I.M. Tiginyanu, L. Chow, L.K. Ono, B. Roldan Cuenya, H. Heinrich, E.E. Yakimov, Synthesis and characterization of ZnO nanowires for nanosensor applications, Materials Research Bulletin 45 (2010) 1026–1032.

[50] J. Goldberger, D.J. Sirbuly, M. Law, P. Yang, ZnO nanowire transistors, Journal of Physical Chemistry B 109 (1) (2005) 9–14.

[51] Z. Chen, C. Lu, Humidity sensors: a review of materials and mechanisms, Sensor Letters 3 (2005) 274–295.

[52] G.Y. Chai, L. Chow, O. Lupan, E. Rusu, G.I. Stratan, H. Heinrich, V.V. Ursaki, I.M. Tiginyanu, Fabrication and characterization of an individual ZnO microwire-based UV photodetector, Solid State Sciences 13 (2011) 1205–1210.

[53] E. Traversa, A. Bearzotti, A novel humidity-detection mechanism for ZnO dense pellets, Sensors and Actuators B 23 (1995) 181–186.

[54] J.D. Prades, R. Jimenez-Diaz, F. Hernandez-Ramirez, A. Cirera, A. Romano-Rodriguez, J.R. Morante, An experimental method to estimate the temperature of individual nanowires, International Journal of Nanotechnology 2009 (2009) 783675.

[55] J.D. Prades, R. Jimenez-Diaz, F. Hernandez-Ramirez, A. Cirera, A. Romano-Rodriguez, J.R. Morante, Harnessing self-heating in nanowires for energy efficient, fully autonomous and ultra-fast gas sensors, Sensors and Actuators B 144 (2010) 1–5;
(b) J.D. Prades, R. Jimenez-Diaz, F. Hernandez-Ramirez, S. Barth, A. Cirera, A. Romano-Rodriguez, S. Mathur, J.R. Morante, Ultralow power consumption gas sensors based on self-heated individual nanowires, Applied Physics Letters 93 (2008) 123110.

[56] H. Fangohr, D.S. Chernyshenko, M. Franchin, Th. Fischbacher, G. Meier, Joule heating in nanowires, Physical Review B 84 (2011) 054437.

[57] M.-H. Wang, K.-A. Hu, B.-Y. Zhao, N.-F. Zhang, Degradation phenomena due to humidity in low voltage ZnO varistors, Ceramics International 33 (2007) 151–154.

[58] W. Kim, G. Kwak, M. Jung, S.K. Jo, J.B. Miller, A.J. Gellman, K. Yong, Surface and internal reactions of ZnO nanowires: etching and bulk defect passivation by H atoms, Journal of Physical Chemistry C 116 (2012) 16093–16097.

[59] Y. Wang, B. Meyer, X. Yin, M. Kunat, D. Langenberg, F. Traeger, A. Birkner, C. Wöll, Physical Review Letters 95 (2005) 266104.

[60] L. Chan, G.L. Griffin, Temperature programmed desorption studies of hydrogen on Zn (0 0 0 1) surfaces, Surface Science 145 (1984) 185–196.

[61] B. Roldan Cuenya, A. Kolmakov, Nanostructures: Sensor and Catalytic Properties, Functional Nanostructures Nanostructure Science and Technology (2008) 305–344, http://dx.doi.org/10.1007/978-0-387-48805-9_6.

[62] Z. Fan, D. Wang, P.C. Chang, W.Y. Tseng, J.G. Lu, ZnO nanowire field-effect transistor and oxygen sensing property, Applied Physics Letters 85 (2004) 5923.
[63] M. Zhao, X. Wang, L. Ning, J. Jia, X. Li, L. Cao, Electrospun Cu-doped ZnO nanofibers for $H_2S$ sensing, Sensors and Actuators B 156 (2011) 588–592.
[64] Z. Fan, J.G. Lu, Electrical properties of ZnO nanowire field effect transistors characterized with scanning probes, Applied Physics Letters 86 (2005) 032111.
[65] Y. Zhang, A. Kolmakov, Y. Lilach, M. Moskovits, Electronic control of chemistry and catalysis at the surface of an individual tin oxide nanowire, Journal of Physical Chemistry B 109 (2005) 1923–1929.
[66] J. Zhou, Y. Gu, Y. Hu, W. Mai, P.H. Yeh, G. Bao, A.K. Sood, D.L. Polla, Z.L. Wang, Gigantic enhancement in response and reset time of ZnO UV nanosensor by utilizing Schottky contact and surface functionalization, Applied Physics Letters 94 (2009) 191103.
[67] Q. Kuang, C.S. Lao, Z. Li, Y.Z. Liu, Z.X. Xie, L.S. Zheng, Z.L. Wang, Enhancing the photon- and gas-sensing properties of a single $SnO_2$ nanowire based nanodevice by nanoparticle surface functionalization, Journal of Physical Chemistry C 112 (30) (2008) 11539–11544.
[68] T.Y. Wei, P.H. Yeh, S.Y. Lu, Z.L. Wang, Gigantic enhancement in sensitivity using schottky contacted nanowire nanosensor, Journal of the American Chemical Society 131 (2009) 17690–17695.
[69] G.Y. Chai, O. Lupan, E.V. Rusu, G.I. Stratan, V.V. Ursaki, V. Şontea, H. Khallaf, L. Chow, Functionalized individual ZnO microwire for natural gas detection, Sensors and Actuators A 176 (2012) 64–71.
[70] A. Zangwill, Physics at Surfaces, Cambridge University Press, Cambridge, 1988.
[71] C.W. Sun, P. Xin, C.Y. Ma, Z.W. Liu, Q.Y. Zhang, Y.Q. Wang, Z.J. Yin, S. Huang, T. Chen, Optical and electrical properties of $Zn_{1-x}Cd_xO$ films grown on Si substrates by reactive radio-frequency magnetron sputtering, Applied Physics Letters 89 (2006) 181923.
[72] X. Tang, H. Lü, Q. Zhang, J. Zhao, Y. Lin, Study on interactions between cadmium and defects in Cd-doped ZnO by first-principle calculations, Solid State Sciences 13 (2011) 384–387.
[73] According to the specifications given by the manufacturer (European Aeronautic Defense and Space Company, EADS N.V.), the suspended membranes model IESSICA require 140 mW to reach the maximum temperature achieved with self-heating ($I_{m\,max}$ = 300 nA corresponded to $T \gg 300\,^{\circ}C$).

## Biographies

**Oleg Lupan** received his M.S. in microelectronics and semiconductor devices from the Technical University of Moldova (TUM) in 1993. He received his Ph.D. in solid state electronics, microelectronics and nanoelectronics from the Institute of Applied Physics, Academy of Sciences of Moldova (ASM) in 2005. His post-doctorate research activities were carried out at the French CNRS, Paris, France and the University of Central Florida, USA. He received his doctor habilitate degree in 2011 from the Institute of Electronic Engineering and Nanotechnologies of ASM. He is an Associate Professor and researcher scientist in solid state electronics, microelectronics and nanoelectronics at the Department of Microelectronics and Semiconductor Devices of the TUM. His current research interests include sensors, optoelectronic devices, nanotechnologies and nanodevices.

**Lee Chow** is a Professor at the Department of Physics of the University of Central Florida in Orlando (USA). He received his B.S. in physics in 1972 from the National Central University, Taiwan. He received a Ph.D. in Physics from Clark University, Worcester, MA, USA in 1981. In 1981–1982 he was a postdoc in the Physics Department at the University of North Carolina, Chapel Hill, NC. He joined the University of Central Florida in 1983 as an assistant Professor, and was promoted to associate professor in 1988 and to professor in 1998. His areas of expertise are: chemical bath deposition, nanofabrications of carbon nanotubes and metal oxides, diffusion in semiconductors, high $T_c$ thin film, hyperfine interactions, high pressure physics, and thin films.

**Thierry Pauporté** is the director of research at the Centre National de la Recherché Scientifique (CNRS) in France. He graduated in Chemistry from the École Normale Supérieure of Lyon. He received his Ph.D. in physical chemistry from Montpellier II University (France) in 1995. Dr. Pauporté has made original and innovative contributions to the synthesis, characterization and understanding of fundamental chemical and physical properties of oxide films and nanostructures. He is also interested in a variety of oxide materials prepared in his group (ZnO, $TiO_2$, $WO_3$, $ZrO_2$, CoOOH, $Co_3O_4$, $Fe_2O_3$, $Fe_3O_4$, $Eu_2O_3$, $Er_2O_3$, etc.). He is also interested in the functionalization of oxide surfaces. He works on the integration of films and structures in efficient devices and their applications (LED, photovoltaic solar cells, photocatalysis, wettability, fouling, etc.).

**Luis Katsuya Ono** is currently a post-doctoral scholar at the Interdisciplinary Nanoscience Center at Aarhus University in Denmark. He obtained a B.S. in Physics/Microelectronics in 2000 at the University of Sao Paulo (Brazil), a M.S in Nuclear Engineering at Kyoto University (Japan), and a Ph.D. in Physics in 2009 at the University of Central Florida (USA) for his investigations of the catalytic properties of metal nanoparticles.

**Beatriz Roldan Cuenya** is a professor in the Department of Physics at the University of Central Florida (UCF) in Orlando (USA). She joined UCF in 2004 after her post-doctoral research in the Department of Chemical Engineering at the University of California Santa Barbara (2001–2003). She obtained her Ph.D. from the Department of Physics at the University of Duisburg-Essen (Germany) summa cum laude in 2001. She completed her M.S./B.S. in Physics with a minor in Materials Science from the University of Oviedo, Spain in 1998. Her research program explores novel physical and chemical properties of size- and shape-selected nanostructures, with emphasis on advancements in nanocatalysis.

**Guangyu Chai** is the Research Director at Apollo Technologies, Inc., Orlando, FL, USA. He received his B.S. in physics in 1999 from the Peking University, Beijing, China. He received a Ph.D. in Condensed Matter Physics from University of Central Florida, Orlando, FL, USA in 2004. His research interests include ZnO nanorod sensors, Individual carbon nanotube devices, and focused ion beam fabrication of nanodevices.